Optical Properties of the (CrF(6))(3-) Complex in A(2)BMF(6):Cr(3+) Elpasolite Crystals: Variation with M-F Bond Distance and Hydrostatic Pressure

ARTICLE *in* INORGANIC CHEMISTRY · OCTOBER 2008

Impact Factor: 4.76 · DOI: 10.1021/ic800606h · Source: PubMed

3 AUTHORS, INCLUDING:

Fernando Rodríguez
Universidad de Cantabria
178 PUBLICATIONS **1,335** CITATIONS

Article

Optical Properties of the $(CrF)^{-}$ Complex in ABMF:Cr^{+} Elpasolite Crystals: Variation with M#F Bond Distance and Hydrostatic Pressure

Ignacio Herna#ndez, Fernando Rodri#guez, and Alain Tressaud

Inorg. Chem., **2008**, 47 (22), 10288-10298 • Publication Date (Web): 21 October 2008

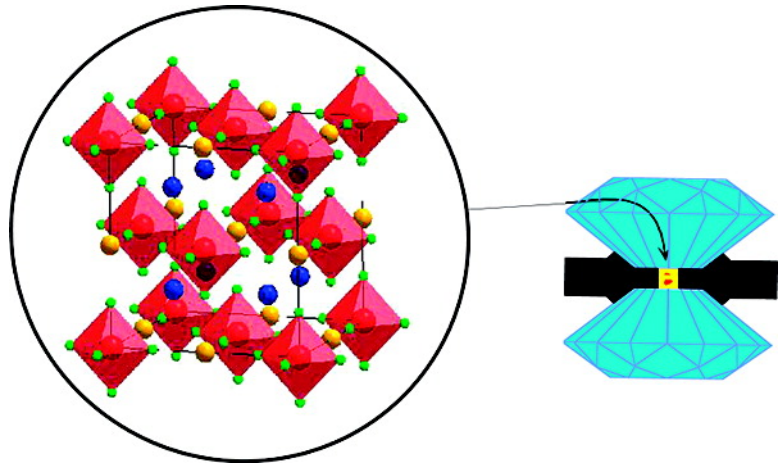

Inorg. Chem. **2008**, *47*, 10288−10298

Optical Properties of the $(CrF_6)^{3-}$ Complex in $A_2BMF_6:Cr^{3+}$ Elpasolite Crystals: Variation with M−F Bond Distance and Hydrostatic Pressure

Ignacio Hernández,[†] Fernando Rodríguez,*[,†] and Alain Tressaud[‡]

MALTA CONSOLIDER Team, DCITIMAC, Facultad de Ciencias, Universidad de Cantabria, 39005 Santander, Spain, and ICMCB-CNRS, Ave. Dr. A. Schweitzer, 33608 Pessac Cedex, France

Received April 4, 2008

This work investigates the photoluminescence (PL) properties of the Cr^{3+}-doped and Cr^{3+}-pure fluoroelpasolites along the A_2BMF_6 series and as a function of pressure. In particular, we focus on the variation of the crystal-field spectrum and the associated PL. The results are explained on the basis of the octahedral $(CrF_6)^{3-}$ complex subjected either to external pressure or the internal pressure exerted by different crystal hosts. We have established structural correlations between the crystal-field parameter 10Dq and the Cr−F distance, R_{Cr-F}, from which we have determined the local structure around the Cr^{3+} impurity, allowing the host material effect on the Cr−F bonds to be studied. As salient features, we show, first, a weak dependence of the first excitation energy, E_1, usually identified as 10Dq, with R_{Cr-F} as $E_1 = KR_{Cr-F}^{-3.3}$, and, second, an increase of the Stokes shift upon R_{Cr-F} reduction or with increasing pressure. We associate this unusual behavior with the existence of state mixing among $^4T_{2g}(F)$, $^2E_g(G)$, and $^2T_{1g}(G)$ states in the first excitation band of Cr^{3+}. Finally, high-pressure experiments performed on Rb_2KCrF_6 indicate that the excited-state spin crossover, $^2E_g(G) \leftrightarrow {}^4T_{2g}(F)$, takes place around 7 GPa. The results indicate the suitability of the selected $A_2BMF_6:Cr^{3+}$ elpasolites to establish structural correlations between PL and R_{Cr-F}.

I. Introduction

There has been a great deal of work focusing on the photoluminescence (PL) properties of Cr^{3+}-doped crystals and glasses.[1−25] The uses of $LiCaAlF_6:Cr^{3+}$ as a laser material[6,7] and $LiSrAlF_6:Cr^{3+}$ for fiber amplifiers[8,9] are illustrative examples of the interest for their use in applications. Among fluoride crystals, elpasolites have received particular attention due to their simple cubic structure and the isolated character of $(CrF_6)^{3-}$ complexes, which do not share any common F ligand in the elpasolite structure.[26,27] Fluorides are usually employed as ideal host lattices for accommodating di- and trivalent cations in perfect octahedral sites (M) due to the large variety of cubic crystals with the perovskite (AMF_3)[28−32] and elpasolite (A_2BMF_6)[10−20,30,33−35] structures, respectively. Our research focuses on the optical absorption/excitation, PL, and excited-state crossover (ESCO) phenomena in the $(CrF_6)^{3-}$ complex, and their dependence on the Cr−F bond distance. Although

* Author to whom correspondence should be addressed. E-mail: rodriguf@unican.es.
† Universidad de Cantabria.
‡ ICMCB-CNRS.

(1) Bray, K. L. *Top. Curr. Chem.* **2001**, *213*, 1.
(2) Grinberg, M. *Opt. Mater.* **2002**, *19*, 37.
(3) Kobyakov, S.; Suchocki, A.; Arizmendi, L.; Jaque, F. *Appl. Phys. Lett.* **2008**, *92*, 071904.
(4) Illarramendi, M. A.; Balda, R.; Fernández, J. *Phys. Rev. B: Condens. Matter Mater. Phys.* **1993**, *47*, 8411.
(5) Lipinska-Kalita, K. E.; Krol, D. M.; Hemley, R. J.; Kalita, P. E.; Gobin, C. L.; Ohki, Y. *J. Appl. Phys.* **2005**, *98*, 054302.
(6) Payne, S. A.; Chase, L. L.; Newkirk, H. W.; Smith, L. K.; Krupke, W. F.; IEEE, J. *Quant. Electron.* **1988**, *24*, 2243.
(7) Lee, H. W. H.; Payne, S. A.; Chase, L. L. *Phys. Rev. B: Condens. Matter Mater. Phys.* **1989**, *39*, 8907.
(8) Payne, S. A.; Chase, L. L.; Smith, L. K.; Kway, W. L.; Newkirk, H. W. *J. Appl. Phys.* **1989**, *66*, 1051.
(9) Barry, N. P.; Hyde, S. C. W.; Mellish, R.; French, P. M. W.; Taylor, J. R.; van der Poel, C. J.; Valster, A. *Electron. Lett.* **1994**, *30*, 1761.
(10) Ferguson, J.; Guggenheim, H. J.; Wood, D. L. *J. Chem. Phys.* **1971**, *54*, 504.
(11) Dolan, J. F.; Kappers, L. A.; Bartram, R. H. *Phys. Rev. B: Condens. Matter Mater. Phys.* **1986**, *33*, 7339.
(12) Bartram, R. H.; Charpie, J. C.; rews, L. J.; Lempicki, A. *Phys. Rev. B: Condens. Matter Mater. Phys.* **1986**, *34*, 2741.
(13) Marco de Lucas, M. C.; Rodriguez, F.; Dance, J. M.; Moreno, M.; Tressaud, A. *J. Lumin.* **1991**, *48/49*, 553.
(14) Dolan, F.; Rinzler, A. G.; Kappers, L. A.; Bartram, R. H. *J. Phys. Chem. Solids* **1992**, *53*, 905.
(15) Woods, A. M.; Sinkovits, R. S.; Charpie, J. C.; Huang, W. L.; Bartram, R. H.; Rossi, A. R. *J. Phys. Chem. Solids* **1993**, *54*, 543.
(16) Marco de Lucas, M. C.; Dance, J. M.; Rodriguez, F.; Tressaud, A.; Moreno, M.; Grannec, J. *Radiat. Eff. Defects Solids* **1995**, *135*, 19.
(17) da Fonseca, R. J. M., Jr; Silva, P. S.; Abritta, T.; Khaidukov, N. M. *Sol. Stat. Commun.* **1999**, *110*, 519.
(18) Sosman, L. P., Jr; da Fonseca, R. J. M.; Abritta, T.; Khaidukov, N. M. *Sol. Stat. Commun.* **2000**, *114*, 661.

10.1021/ic800606h CCC: $40.75
Published on Web 10/21/2008

correlations between the PL and the host M−X (X = Cl, F, O, N) distance have been previously established,[19] a correlation study between optical properties and the actual Cr−F bond distance, R_{Cr-F}, is absent. Preliminary studies on $K_2NaScF_6:Cr^{3+}$ and $K_2NaGaF_6:Cr^{3+}$ using high-pressure spectroscopy[11,14,15] and ab initio calculations[14,15,20] were aimed at correlating the optical properties with the local structure of $(CrF_6)^{3-}$ in these impurity systems. This is, however, hard to establish in impurity systems, due to difficulty in determining R_{Cr-F} precisely. This feature makes pure A_2BCrF_6 systems attractive for establishing correlations between the optical properties and the structure, which is crucial for a microscopic understanding of the PL properties.

The present work investigates the PL properties of the doped impurity elpasolite systems $Rb_2KGaF_6:Cr^{3+}$, $K_2NaGaF_6:Cr^{3+}$, and $Rb_2KInF_6:Cr^{3+}$ and Cr-pure Rb_2KCrF_6 and Tl_2KCrF_6 as a function of the host crystal structure and the local structure around Cr^{3+}. Such a crystal series makes reliable opto-structural correlation studies employing a systematic methodology possible. This procedure becomes necessary given that there is significant variation of the reported metal−fluorine distance, R_{M-F}, for some crystals of the series.[35−39] Accordingly, we provide combined powder X-ray diffraction (XRD) and, Raman and optical spectroscopy data, the analyses of which have been performed systematically for the whole A_2BMF_6 series. This method provides a reliable set of bond distances and optical parameters. Attention is paid to the variation of the excitation and the corresponding PL spectra with R_{Cr-F}. The results are compared with those obtained in similar Cr^{3+}-doped systems and are explained by a crystal-field (CF) model of the electronic structure of the complex anion and its electron−phonon coupling. Pressure experiments performed on Rb_2KCrF_6 around the ESCO complement the correlation study and enable us to compare the variation in the optical properties induced by volume changes. The PL transformation occurring above the ESCO pressure in the Cr-pure Rb_2KCrF_6 elpasolite is studied and compared with previous results obtained in Cr-doped fluoroelpasolites[11] and garnets.[1,2]

II. Experimental Section

Single-crystal elpasolites of K_2NaGaF_6, Rb_2KGaF_6, and Rb_2KInF_6 doped with 1 mol % of CrF_3 as well as single crystals of Rb_2KCrF_6 and Tl_2KCrF_6 were grown by the Bridgman technique[40] according to a procedure described elsewhere.[13,35] The elpasolite structure ($Fm\bar{3}m$) of the crystal series at ambient conditions was checked by XRD using a Bruker D8 Advance. XRD diagrams, $I(2\theta)$, were obtained at $T = 290$ K for each crystal and analyzed through the Fullprof program package.[41] The same procedure for sample preparation, data acquisition, and fitting analysis was employed for the whole series. Although the method can involve systematic errors in the bond distance determination analogously to other previous reports,[35−39] the precision for determining bond distance variation in the series is significantly improved. The Raman spectra were obtained on single crystals using a Ramanor U-1000 double spectrometer equipped with a Symphony CCD in a confocal microscope. The Raman peaks corresponding to the breathing a_{1g} mode of the $(CrF_6)^{3-}$ were compared with R_{Cr-F} obtained in the pure crystals in order to obtain the local Grüneisen parameter for this vibrational mode. This procedure allows us to probe R_{Cr-F} in impurity systems through the a_{1g} frequency obtained from the vibronic side bands of the low-temperature PL spectra.[10,11,13,14]

The excitation and emission spectra at ambient conditions were obtained by means of a Fluoromax-2 fluorometer attached with suitable interference filters to improve the quality of the spectra. The excitation and emission spectra were corrected for instrumental response. For low-temperature spectra, a Scientific Instruments 202 cryostat equipped with an APD-K temperature controller was used. The pressure experiments in Rb_2KCrF_6 were done in a Diamond anvil cell (Diamond Optics Inc.) using a 16:4:1 methanol−ethanol−water mixture as a pressure transmitter. The pressure was calibrated from the Ruby R-line shift. In both cases, the emission spectra under pressure were obtained using an adapted microspectrometer setup described elsewhere.[42,43] For high-pressure excitation spectroscopy, the Fluoromax-2 fluorometer was adapted for microscope operation. PL was excited with a Coherent Krypton laser model Innova 300. For room-temperature absorption and emission, the spectral resolution was 1 nm. At low temperatures and in Raman experiments, the spectral resolution was 0.1 nm. The PL lifetime of Cr^{3+} was measured from the time-dependent intensity, $I(t)$, under chopped excitation using a Neos Technologies 35085 acousto-optic modulator. $I(t)$ was recorded with a Hamamatsu R928 photomultiplier and a Tektronix 2430 A oscilloscope.

(19) Tanner, P. A. *Chem. Phys. Lett.* **2004**, *388*, 488.
(20) Pueyo, L.; Richardson, J. W. *J. Chem. Phys.* **1977**, *67*, 3583.
(21) Greenough, H.; Paulusz, A. G. *J. Chem. Phys.* **1979**, *70*, 1967.
(22) Drickamer G., Frank C. W. *Electronic Transitions and the High Pressure Chemistry and Physics of Solids*; Chapman & Hall: London, 1973.
(23) Knochenmuss, R.; Reber, C.; Rajasekharan, M. V.; Güdel, H. U. *J. Chem. Phys.* **1986**, *85*, 4280.
(24) Wenger, O.; Güdel, H. U. *J. Chem. Phys.* **2001**, *114*, 5832.
(25) Wenger, O.; Valiente, R.; Güdel, H. U. *J. Chem. Phys.* **2001**, *115*, 3819.
(26) Nakajima, T.; Zemva, B.; Tressaud, A. *Advanced Inorganic Fluorides: Synthesis, Characterization and Applications*: Elsevier Science & Technology, 2000.
(27) Flerov, I. N.; Goreva, M. V.; Grannec, J.; Tressaud, A. *J. Fluorine Chem.* **2002**, *116*, 9.
(28) Rodríguez, F.; Moreno, M. *J. Chem. Phys.* **1986**, *84*, 692.
(29) Rodríguez, F.; Moreno, M.; Tressaud, A.; Chaminade, J. P. *Cryst. Lattice Defects Amorphous Mater.* **1987**, *16*, 221.
(30) Rodríguez, F.; Moreno, M.; Dance, J. M.; Tressaud, A. *Solid State Commun.* **1989**, *69*, 67.
(31) Rodríguez, F.; Riesen, H.; Güdel, H. U. *J. Lumin.* **1991**, *50*, 101.
(32) Marco de Lucas, M. C.; Rodríguez, F.; Moreno, M. *Phys. Rev. B: Condens. Matter Mater. Phys.* **1994**, *50*, 2760.
(33) Kuze, S.; du Boulay, D.; Ishizawa, N.; Kodama, N.; Yamaga, M.; Henderson, B. *J. Sol. Stat. Chem.* **2004**, *177*, 350.
(34) Grzechnik, A.; Dmitriev, V.; Weber, H. P.; Gesland, J. Y.; van Smaalen, S. *J. Phys.: Condens. Matter* **2004**, *16*, 1033.
(35) Guengard, H. Ph.D. thesis, University of Bordeaux 1, Bordeaux, France, 1994.
(36) Knox, K. *J. Inorg. Nucl. Chem.* **1961**, *21*, 253.
(37) Schneider, S. *Z. Anorg. Allg. Chem.* **1970**, *376*, 268.
(38) Massa, W. *Rev. Chim. Miner.* **1986**, *23*, 508.
(39) Reber, C.; Güdel, H. U.; Meyer, G.; Schtied, T.; Daul, C. A. *Inorg. Chem.* **1989**, *28*, 3249.
(40) *The Development of Crystal Growth*; Scheel, H. J., Fukuda, T., Eds; John Wiley: New York, 2003.
(41) Rodriguez-Carvajal, J. *Physica B* **1993**, *192*, 55.
(42) Garcia-Revilla, S.; Rodriguez, F.; Valiente, R.; Pollnau, M. *J. Phys.: Condens. Matter* **2002**, *14*, 447.
(43) Hernández, I.; Rodríguez, F. *Phys. Rev. B: Condens. Matter Mater. Phys.* **2003**, *67*, 012101.

Table 1. Structural Data Obtained from (a) X-Ray Diffraction for A_2BMF_6 Fluoroelpasolite, Space Group $Fm\bar{3}m$,[a] and (b) Vibrational Frequencies, $\omega_{a_{1g}}$, from Raman and Just from the Low-Temperature Emission Spectra in K_2NaCrF_6, Rb_2KCrF_6, and Tl_2KCrF_6, and the Emission Spectra in Cr^{3+}-Doped Fluoroelpasolites[b]

Part a

	present work			previous works			
	a (Å)	x_F	R_{M-F} (Å)	a (Å)	x_F	R_{M-F} (Å)	ref
K_2NaAlF_6				8.093	0.222	1.80	37
K_2NaCrF_6				8.275	0.2293	1.897	38
K_2NaGaF_6	8.255	0.228	1.88	8.257	0.227	1.874	35
K_2NaScF_6				8.4717	0.2342	1.984	39
Rb_2KCrF_6	8.825	0.215	1.90	8.827	0.213	1.88	35
Rb_2KGaF_6	8.820	0.214	1.89	8.817	0.214	1.89	35
Rb_2KInF_6	9.110	0.220	2.00	9.098	0.222	2.02	35
Tl_2KCrF_6	8.835	0.219	1.93				

Part b

		R_{Cr-F} (Å)	
	$\hbar\omega_{a1g}$ (cm^{-1})	a_{1g}	XRD
K_2NaCrF_6	570 ± 2	1.897 ± 0.001*	1.897 ± 0.001
Rb_2KCrF_6	545 ± 2	1.912 ± 0.003	1.90 ± 0.01
Tl_2KCrF_6	536 ± 2	1.920 ± 0.003	1.93 ± 0.01
$K_2NaAlF_6:Cr^{3+}$	575 ± 2	1.895 ± 0.003	
$K_2NaGaF_6:Cr^{3+}$	568 ± 2	1.899 ± 0.003	
$Rb_2KGaF_6:Cr^{3+}$	556 ± 2	1.906 ± 0.003	

[a] Parameters a, x_F, and R_{M-F} denote the lattice parameter, the F^- coordinate in the unit cell, and the M−F bond length, respectively, determined in the present work as well as in the attached references. [b] R_{Cr-F} was derived from $\omega_{a_{1g}}$ through eq 9: $R_{Cr-F} = k'(\omega_{a_{1g}})^{-1/3\gamma}$ with $\gamma = 2.1$ and $k' = (1/k)^{-1/3\gamma} = 5.195$. Units in angstroms and cm^{-1}, respectively. See text.

III. Results and Discussion

A. Structural Study: Determination of R_{Cr-F} in $A_2BMF_6:Cr^{3+}$. The XRD patterns of K_2NaGaF_6, Rb_2KGaF_6, and Rb_2KInF_6 doped with 1 mol % of CrF_3 as well as Rb_2KCrF_6 and Tl_2KCrF_6 correspond to the cubic elpasolite structure. The relevant structural parameters obtained from $I(2\theta)$ with the Fullprof software[41] are given in Table 1a together with previously reported data. The present data provide a precise distance variation along the series since all XRD diagrams and analyses were done following the same procedure. Figure 1 shows the elpasolite structure and the local CrF_6^{3-} complex a_{1g} vibrational mode, whose frequency was measured by Raman spectroscopy at room temperature, and from the vibrational structure of the PL spectra at low temperatures. Table 1b collects the vibrational frequencies and the corresponding R_{Cr-F} for the Cr-pure elpasolites obtained from XRD and also from the equation $\omega_{a_{1g}} = kR_{Cr-F}^{-3\gamma_{loc}}$ (refs14, 15, and 32). We have employed a local Grüneisen parameter $\gamma_{loc} = 2.1$, derived for the $(CrF_6)^{3-}$ complex embedded in elpasolites,[14,15,37,44] and $k = 3.22 \times 10^4$ (cm^{-1} $Å^{1/3\gamma}$), determined from the K_2NaCrF_6 frequency and Cr−F distance, which were measured with high precision by Ferguson et al. and Massa, respectively.[10,38] A survey of vibrational frequencies for Cr^{3+} in different elpasolites is collected elsewhere.[19]

B. Spectroscopic Properties along the Elpasolite Series. B.1. Fano Resonance. All of the A_2BMF_6 crystals investigated in this work are luminescent at room temperature under excitation in the Cr^{3+} absorption bands. Their excitation and emission spectra at room temperature are shown in Figure 2. For pure compounds, we report the optical absorption (OA) spectra instead of the excitation spectra given that the excitation band shape appears somewhat distorted due to the crystal absorptivity. The three excitation or OA bands placed around 2.0, 2.7, and 4.3 eV are assigned within O_h-symmetry $(CrF_6)^{3-}$ to electronic crystal-field transitions from the $^4A_{2g}(F)$ ground state to the $^4T_{2g}(F)$, $^4T_{1g}(F)$, and $^4T_{1g}(P)$ excited states, respectively, according to the Tanabe−Sugano diagram for d^3 ions (Figure 3).[45,46] Note that the energy of the first ($^4A_{2g} \rightarrow {}^4T_{2g}$) excitation energy coincides with 10Dq. However, it is worth noting the triplet structure exhibited by the first band in the OA spectrum, which is associated with the mixing of the $^4T_{2g}(F)$, $^2E_g(G)$, and $^2T_{1g}(G)$ by the spin−orbit interaction (Fano resonances). The CF parameter, 10Dq, obtained from the OA spectrum is close to the ESCO point, $(10Dq/B)_{ESCO} = 20$, and thus these states are significantly coupled by the spin−orbit interaction (Figure 3). Each state shows the highest coupling at the intersection point of the Tanabe−Sugano diagram, and their energy is calculated as a function of $10Dq/B$ for a given value of C/B, where B and C are the Racah parameters.[45,46] Such couplings are seen in the absorption spectra as protuberances (Fano resonance) or small dips (Fano antiresonance)[47−49] at the crossing energy of $^4T_{2g}(F) \leftrightarrow {}^2E_g(G)$ and $^4T_{2g}(F) \leftrightarrow {}^2T_{1g}(G)$ states, respectively (Figure 4). Given that these features appear around the maximum of the $^4T_{2g}(F)$ absorption band in Cr^{3+}-doped fluoroelpasolites (Figure 2), the determination of 10Dq as derived from the band maximum is complicated. If we define E_1 as the first-order moment, M1, of the first absorption band, which corresponds to the band maximum in single Gaussian-shaped bands, then the CF parameter 10Dq = 2.0 eV is given approximately by $E_1 \approx 10Dq$, for Cr^{3+}. However, due to the presence of Fano resonances, its variation with R_{Cr-F} may be not the same as 10Dq: $\partial E_1/\partial R_{Cr-F} \neq \partial 10Dq/\partial R_{Cr-F}$. According to the Tanabe−Sugano diagram for octahedral Cr^{3+} ($3d^3$) in Figure 3, E_1 is expected to vary as $E_1 = 10Dq$ for CF values far from ESCO. On the other hand, near ESCO, E_1 may behave somewhat differently than 10Dq. In fact, it can be easily shown that variation of E_1 with R_{Cr-F} is either lower or higher than the variation of 10Dq with R_{Cr-F} provided that we deal with Fano antiresonance or Fano resonance, respectively. If we denote by α_1 and α_2 the fractions of the band intensity deviations from the

(44) Francisco, E.; Flórez, M.; Barandiarán, Z.; Fernández Rodrigo, G.; Luaña, V.; Recio, J. M.; Bermejo, M.; Seijo, L.; Pueyo, L. *Cryst. Lattice Defects Amorphous Mater.* **1987**, *15*, 45.

(45) Tanabe, Y.; Sugano, S. *J. Phys. Soc. Jpn.* **1954**, *9*, 753.
(46) Griffith, J. S. *The Theory of Transition-Metal Ions*; Cambridge University Press: Cambridge, U.K., 1980.
(47) Fano, U. *Phys. Rev.* **1961**, *124*, 1866.
(48) Sturge, M. D.; Guggenheim, H. J.; Pryce, M. H. L. *Phys. Rev. B: Condens. Matter Mater. Phys.* **1970**, *7*, 2459.
(49) Ley, L.; Kärcher, R.; Johnson, R. L. *Phys. Rev. Lett.* **1984**, *53*, 710.

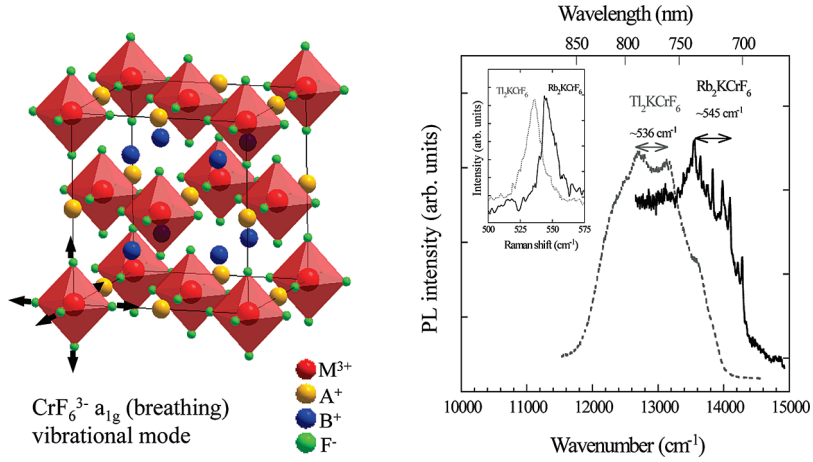

Figure 1. (a) Unit cell of the $Fm\bar{3}m$ elpasolite structure A_2BMF_6, showing the normal coordinate corresponding to the a_{1g} mode, which is associated with the totally symmetric mode of the $(MF_6)^{3-}$ octahedron. (b) Emission spectra at $T = 10$ K of the Cr-pure Rb_2KCrF_6 and Tl_2KCrF_6. The inset shows the corresponding Raman spectra around the a_{1g} vibrational mode. Note that both spectra provide nearly the same vibrational energy for each crystal: 67.6 meV (545 cm^{-1}) and 66.5 meV (536 cm^{-1}), respectively.

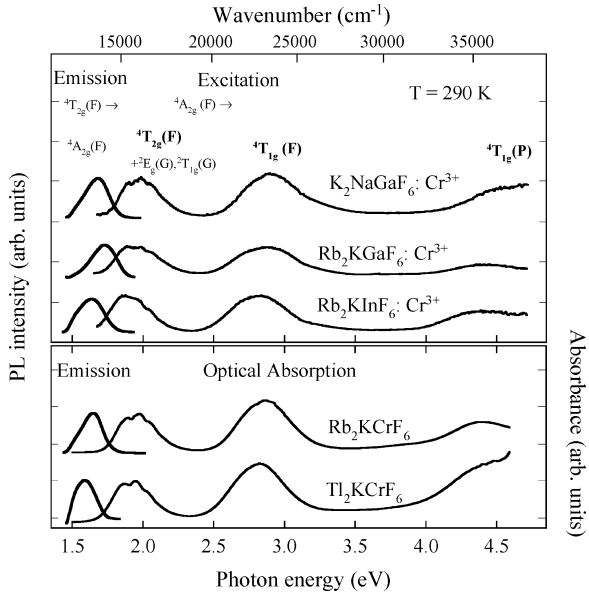

Figure 2. Emission and corresponding excitation/absorption spectra of Cr^{3+}-doped K_2NaGaF_6, Rb_2KGaF_6, and Rb_2KInF_6 as well as Cr^{3+}-pure Rb_2KCrF_6 and Tl_2KCrF_6 at ambient conditions. Bands are identified with the commonly used labels for an octahedral $(CrF_6)^{3-}$ complex.

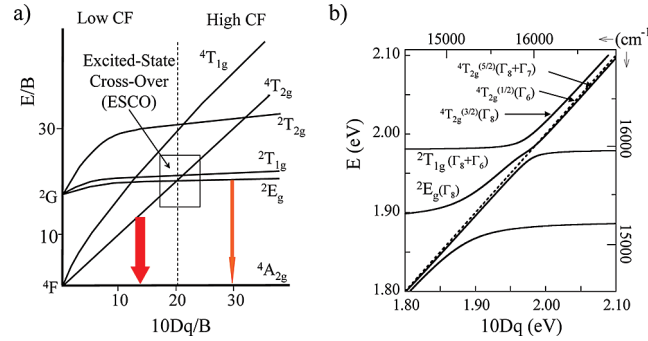

Figure 3. (a) Tanabe−Sugano energy-level diagram emerging from an O_h $3d^3$ configuration (Cr^{3+}). The arrows indicate the two distinct photoluminescence behaviors depending on the crystal field: Broad band emission ($^4T_{2g} \rightarrow {}^4A_{2g}$) for $10Dq < 10Dq_{ESCO}$ and narrow Ruby-like emission ($^2E_g \rightarrow {}^4A_{2g}$) for $10Dq > 10Dq_{ESCO}$. (b) Enlargement of the ESCO point ($10Dq/B = 20$) showing the state mixing induced by spin−orbit interaction. The energies have been calculated using $B = 90$ meV (730 cm^{-1}), $C/B = 4.5$, and $\zeta = 27$ meV (215 cm^{-1}), corresponding to the Racah parameters for Rb_2KCrF_6 and the spin−orbit coupling constant of the Cr^{3+} free ion. Note the different slopes of the spinor energy as a function of $10Dq/B$ for the manifold $^4T_{2g}(F)$, $^2E_g(G)$, and $^2T_{1g}(G)$ states. Γ_i with $i = 6-8$ are the double-group irreps in O_h.

nonresonant absorption band profile of $^4T_{2g}(F)$[47−50] due to resonances between the *narrow* $^2E_g(G)$ and $^2T_{1g}(G)$ states and the *broad* $^4T_{2g}(F)$ state, respectively (Figure 3), then the centroid of the first absorption band, E_1, or the first moment of the band, is given by

$$E_1 = \alpha_1 E(^2E) + \alpha_2 E(^2T_1) + (1 - \alpha_1 - \alpha_2) E(^4T_2) \quad (1)$$

where $E(\Gamma)$ is the energy corresponding to the first moment of the band profile associated with the Γ state. The resonance profiles for $^2E_g(G)$ and $^2T_{1g}(G)$ depend on the coupling parameters with the $^4T_{2g}(F)$ state and have been intensively studied elsewhere.[47−50] For illustrative purposes, Figure 4 depicts several profiles corresponding to different choices of the coupling parameters: they represent what is usually referred to as Fano resonance or Fano antiresonance. In all cases, the first moment of the profile coincides with the energy of the resonant Γ state ($\varepsilon = 0$). According to eq 1, the variation of E_1 with respect to R_{Cr-F} is thus given by

$$\frac{\partial E_1}{\partial R_{Cr-F}} = (1 - \alpha_1 - \alpha_2)\frac{\partial E(^4T_2)}{\partial R_{Cr-F}} = (1 - \alpha_1 - \alpha_2)\frac{\partial 10Dq}{\partial R_{Cr-F}} \quad (2)$$

We have considered that the first two terms are zero since the energy of the $^2E_g(G)$ and $^2T_{1g}(G)$ states are independent of 10Dq to a great extent (Figure 3) and, hence, independent of R_{Cr-F}. However, it is worth noting that this estimate is strictly valid on the assumption that α_1 and α_2 do not change with R_{Cr-F}. Therefore, we conclude from eq 2 that the variation of E_1 with respect to R_{Cr-F} may be either lower or higher than the variation of 10Dq with respect to R_{Cr-F} if $(\alpha_1 + \alpha_2)$ is positive or negative, respectively. The crucial point in such a moment analysis is to elucidate the character

(50) Voda, M.; Garcia Sole, J.; Jaque, F.; Vergara, I.; Kaminskii, A.; Mill, B.; Butashin, A. *Phys. Rev. B: Condens. Matter Mater. Phys.* **1994**, *49*, 3755.

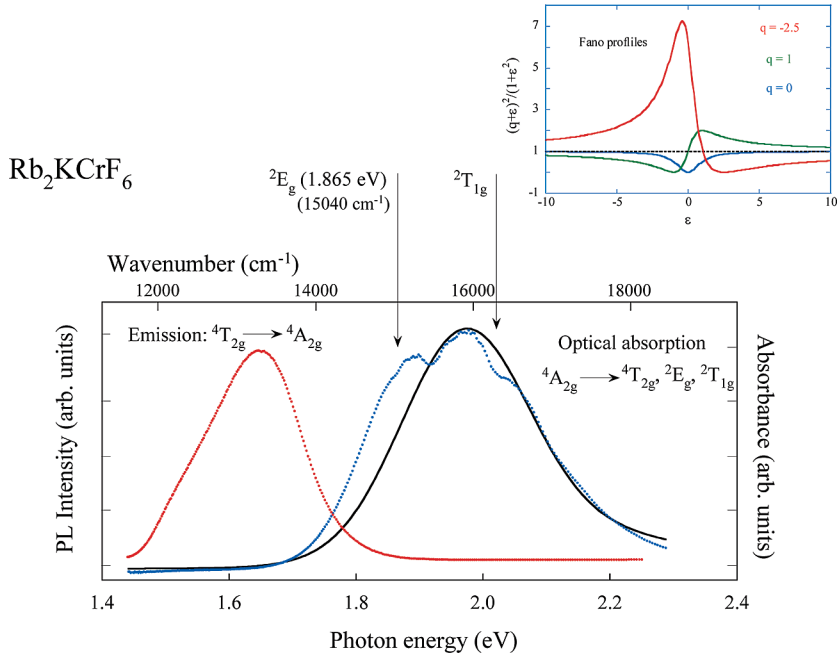

Figure 4. Emission and absorption spectra corresponding to the ($^4T_{2g} \leftrightarrow {}^4A_{2g}$) transition in Rb_2KCrF_6 at ambient conditions. The diplike features at 1.90 and 2.02 eV are associated with Fano resonances between the broad $^4T_{2g}$(F) state and the narrow ^2E_g(G) and $^2T_{1g}$(G) states. The continuous line corresponds to the best two-Gaussian fit to the overall broad band representing the absorption background of the $^4T_{2g}$(F) broad band. The Fano profiles in the upper figure are simulated using eq 3. The ^2E_g energy, $E_0 = 1.865$ eV, obtained from pressure experiments, confirms the character of the $^4T_{2g} \leftrightarrow {}^2E_g$ resonance as a protuberance in the optical spectra. The profile analysis suggests that the $^2T_{1g}$(G) state produces a Fano antiresonance with a dip at 2.02 eV. The calculated Fano profiles account for the observed resonances with relative intensities of 15% for the resonance (^2E_g) and 2% for the antiresonance ($^2T_{1g}$).

of the Fano resonance associated with the ^2E_g(G) and $^2T_{1g}$(G) states. But this is not usually an easy task when the energies of the spin doublets are unknown, since the corresponding peaks are hidden in the optical spectra. In such cases, information on the type of resonance and its associated energy is obtained through band profile analyses.[47−52] Following Fano theory,[47−49] the resonance profile is given by the equation

$$I(\varepsilon) = \frac{(q+\varepsilon)^2}{(1+\varepsilon^2)} = 1 + \frac{q^2 + 2q\varepsilon - 1}{1+\varepsilon^2} \qquad (3)$$

where $\varepsilon = (E - E_0)/\Gamma$ represents a reduced energy scale. Here, E_0 and Γ refer to the energy and width of the resonance, respectively, following the notation used elsewhere.[48−50] The q parameter contains the strength and type of coupling in the resonance. Typical Fano profiles are depicted in Figure 4. The spectral profile ranges from a normal Lorentzian resonance ($|q| \rightarrow \infty$), through a dispersion-like curve ($q = 1$) to an inverted Lorentzian (antiresonance; $0 < q < 1$). Note that the dispersion-like curve corresponds to $I(\varepsilon{=}0) = 0$ in ref 51, since the resonance equation is defined as eq 3 minus 1. Interestingly, these profiles can be distinguished from the optical spectra if we know the energies of the ^2E_g(G) and $^2T_{1g}$(G) resonant states. This knowledge is, though, not straightforward for broadband PL Cr^{3+} systems, the corresponding electronic transitions for which appear as Fano resonances in $^4T_{2g}$(F) (Figure 2). High-pressure experiments performed on Rb_2KCrF_6 in this work (section C) directly provide the energy of ^2E_g(G) as a function of pressure (Figures 5 and 6). Extrapolation of the pressure data provides an energy $E(^2E_g) = 1.865$ eV at ambient conditions. As shown in Figure 4, this value confirms that ^2E_g(G) produces a resonance rather than an antiresonance, as is commonly assumed for this state in many systems.[51,52] The same conclusion was obtained by Garcia-Sole et al. in Cr^{3+}-doped $La_3Ga_{5.5}Nb_{0.5}O_{14}$ and $La_3Ga_{5.5}Ta_{0.5}O_{14}$.[50] On the basis of profile analysis, the authors show that ^2E_g(G) and $^2T_{1g}$(G) give rise to resonance and antiresonance, respectively. A similar analysis has been carried out in Rb_2KCrF_6 (Figure 4), taking advantage of what is known about ^2E_g(G) energy

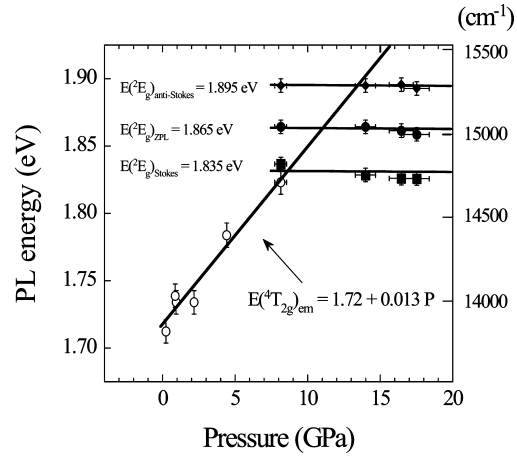

Figure 5. Variation of the Rb_2KCrF_6 emission energy from $^4T_{2g}$ (1.72 eV) and from ^2E_g (1.865 eV) with pressure. The Stokes and anti-Stokes replicas of the $^2E_g \rightarrow {}^4A_{2g}$ lines, as a result of the vibronic coupling with t_{2u} modes with an energy of 30 meV, are also included. The straight lines correspond to the least-squares linear fitting of the experimental data. Note that the intersection point, $E_1 = E_{ZPL}(^2E_g)$, at 11 GPa is different from the ESCO condition: $E_{ZPL}(^4T_{2g}) = E_{ZPL}(^2E_g)$.

(51) Sturge, M. D.; Guggenheim, H. J.; Pryce, M. H. L. *Phys. Rev. B: Condens. Matter Mater. Phys.* **1970**, *2*, 2459.
(52) Kenyon, P.; Andrews, L.; McCollum, B.; Lempicki, A. *J. Quant. Electron. IEEE* **1982**, *18*, 1189.

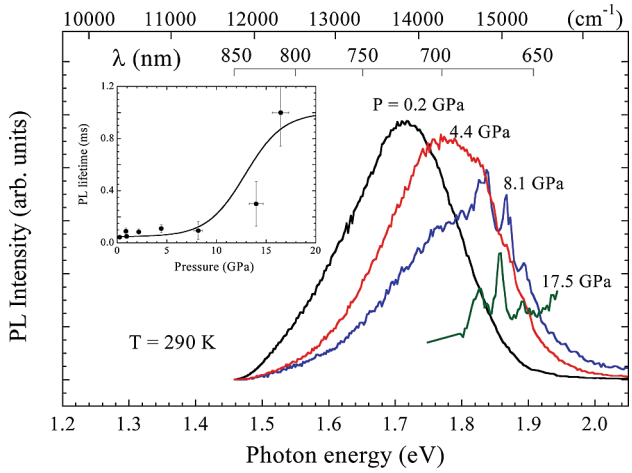

Figure 6. Variation of the emission spectra of Rb_2KCrF_6 as a function of pressure at room temperature upon excitation at 407 nm. The inset shows the corresponding PL lifetime variation. The line represents the calculated lifetime on the basis of two emitting excited states: $^4T_{2g}$ (τ = 45 μs at ambient pressure) and ^2E_g (τ = 1.0 ms at 16.1 GPa). The τ(P) curve was calculated through the equation: τ^{-1} (P) = $(3g_1 + g_2\, e^{\Delta/k_BT})/(3 + e^{\Delta/k_BT})$ using $g_1 = 2.2 \times 10^5$ s$^-$ and $g_2 = 10^3$ s^{-1}, and $\Delta(P) = 0.013P - 0.065$ (see text).

from high-pressure experiments (Figures 5 and 6). According to this, we conclude that ^2E_g(G) resonance produces the major deviation of the absorption background, while $^2T_{1g}$(G) produces an antiresonance with a small deviation (decrease) with respect to the background. The simulations in Figure 4 show that $\alpha_1 \approx 0.15$ and $\alpha_2 \approx -0.02$; therefore, the variation of E_1 with respect to 10Dq, which is given according to eq 2 by $\delta E_1 = (1 - \alpha_1 - \alpha_2)\delta 10\text{Dq} \approx 0.87\delta 10\text{Dq}$, is smaller that the 10Dq variation by about 13%. This noteworthy result must be taken into consideration when discussing R dependences of 10Dq in crystal series and in pressure experiments since the CF value of Cr^{3+} along the series varies from 1.91 to 2.01 eV around ESCO (Table 2), and thus, Fano resonance plays an important role in determining variations of E_1 with respect to crystal volume or pressure.

B.2. Structural Correlations: Dependence on the M−F and Cr−F Distances. For all investigated compounds, the PL spectra consist of a single broad emission band peaking around 1.6 eV, corresponding to the $^4T_{2g}$(F) → $^4A_{2g}$(F) transition. The CF for the excited-state equilibrium geometry lies close to but below ESCO ($^4T_{2g} \leftrightarrow {}^2E_g$), and thus, broadband PL occurs instead of narrow R-line emission (Figures 2−3). It must be pointed out that the actual CF governing PL crossover is given by the excited-state equilibrium Cr−F distance, R^{exc}_{Cr-F}. As Figure 3 shows, $\partial E_1/\partial 10Dq > 0$; then, the linear electron−lattice coupling associated with this transition is negative: $\partial E_1/\partial R_{Cr-F} < 0$, and thus $R^{exc}_{Cr-F} > R^{gr}_{Cr-F}$ for Cr^{3+} (Figure 7). It means that a broad PL band can be observed even if the ground-state CF verifies 10Dq > $(10Dq)_{ESCO}$ (Figure 7a). Note that $(10Dq)_{ESCO}$ given by the Tanabe−Sugano diagram of Figure 3a corresponds to ESCO at the ground-state equilibrium geometry, R^{gr}_{Cr-F} (Q = 0 in Figure 7), but it does not imply a crossover at the energy minima of the corresponding ($^4T_{2g} \leftrightarrow {}^2E_g$) states. According to the configurational energy curves of Figure 7, the latter condition requires zero-phonon lines (ZPL) crossing: $E_{ZPL}(^4T_{2g}) = E_{ZPL}(^2E_g)$. Table 2 collects the experimental transition energies for excitation and emission as well as the calculated energies from the Tanabe−Sugano matrices[45,46] together with the relevant spectroscopic parameters.

The structural effects on the optical properties in the series (chemical pressure) are evidenced through the slight band shifts observed on passing from $K_2NaAlF_6:Cr^{3+}$ (R_{Al-F} = 1.80 Å; 10Dq = 2.01 eV)[21] to $Rb_2KInF_6:Cr^{3+}$ (R_{In-F} = 2.02 Å; 10Dq = 1.92 eV). The difference between these two crystals is noteworthy as regards the variation of 10Dq, which varies only 0.09 eV for $\Delta R_{M-F} = -0.22$ Å. In fact, such a distance variation would induce a larger shift if the variation of the host M−F distance were the same as the impurity Cr−F distance. This is well illustrated in the Cr^{3+}-pure fluoroelpasolites, the 10Dq of which varies from 2.00 eV in Rb_2KCrF_6 (R_{Cr-F} = 1.89 Å) to 1.91 eV in Tl_2KCrF_6 (R_{Cr-F} = 1.93 Å). It means that the same 10Dq variation of 0.09 eV is attained for $\Delta R_{Cr-F} = -0.04$ Å in Cr^{3+}-pure elpasolites, and $\Delta R_{M-F} = -0.22$ Å in Cr^{3+}-doped elpasolites. This difference can be rationalized if we consider lattice relaxation effects around Cr^{3+} in impurity systems. Moreover, the distinct variation of 10Dq with R_{M-F} and R_{Cr-F} clearly suggests that the actual Cr−F distance at the impurity site is close to the sum of the corresponding ionic radii ($R_{Cr-F} \approx R_{Cr^{3+}} + R_{F^-} = 0.62 + 1.33 = 1.95$ Å).[53] An inward or an outward relaxation of the MF_6 octahedron is expected when $R_{M-F} > R_{Cr-F}$ or $R_{M-F} < R_{Cr-F}$, respectively. Similar results were found in Mn^{2+}-doped fluoroperovskites[28,29] and chloroperovskites.[54,55]

The optical data can provide the Cr−F distance for impurity systems if we are able to adequately scale the R_{Cr-F} dependence of 10Dq as

$$10\text{Dq} = KR^{-n}_{Cr-F} \qquad (4)$$

Besides accidental coincidence with the point-charge CF model, n exponents around 5 have been obtained in different transition metal oxide complexes from high-pressure experiments[28,12,22] and from ab initio cluster calculations[15] and other calculation methods[56,57] in $(CrF_6)^{3-}$. Values of n = 4.5 and 4.7 were obtained for $K_2NaGaF_6:Cr^{3+}$ and $K_2NaScF_6:Cr^{3+}$, respectively, whereas n = 4.3 in $(CrF_6)^{3-}$ in vacuo,[44] and n = 4.46 for $Cs_2NaYF_6:Cr^{3+}$ using a fully relativistic discrete variational multielectron method.[57] These values are similar to the n = 4.7 obtained experimentally and from theoretical calculations in Mn^{2+} in fluoroperovskites $AMF_3:Mn^{2+}$.[28,56]

Figure 8 plots the variation of 10Dq obtained by fitting the energies of the absorption bands to the corresponding CF expressions[39] versus R_{Cr-F} for the Cr^{3+}-pure elpasolites.

(53) *Handbook of Chemistry and Physics*, 67th ed; West, R. C., Ed.; CRC Press: Boca Raton, FL, 1997.
(54) Marco de Lucas, M. C.; Rodriguez, F.; Güdel, H. U.; Furer, N. *J. Lumin.* **1994**, *60/61*, 581.
(55) Marco de Lucas, M. C.; Rodriguez, F.; Prieto, C.; Verdaguer, M.; Güdel, H. U. *J. Phys. Chem. Solids* **1995**, *56*, 995.
(56) Moreno, M.; Barriuso, M. T.; Aramburu, J. A. *J. Phys.: Condens. Matter* **1992**, *4*, 9481.
(57) Brik, M. G.; Ogasawara, K. *Phys. Rev. B: Condens. Matter Mater. Phys.* **2006**, *74*, 045105.

Table 2. Emission and Excitation Energies Derived from the Optical Spectra at Room Temperature for the Cr^{3+}-Pure and Cr^{3+}-Doped A_2BMF_6 Fluoroelpasolite Series[a]

	emission	excitation: $^4A_{2g} \rightarrow$						
	$^4T_{2g} \rightarrow {}^4A_{2g}$	$^4T_{2g}(F)$	$^2E_g(G)$	$^4T_{1g}(F)$	$^4T_{1g}(P)$	B	10Dq	ref
$K_2NaAlF_6:Cr^{3+}$	1.67	2.01					2.01 [16210]	21
K_2NaCrF_6		2.00				0.094 [760]	2.00 [16130]	10
$K_2NaGaF_6:Cr^{3+}$	1.67	1.98 (1.98)	(2.33)	2.90 (2.92)	4.56 (4.54)	0.100 [805]	1.98 [15970]	
Rb_2KCrF_6	1.65	1.98 (1.97)	(1.97)	2.88 (2.84)	4.40 (4.42)	0.091 [735]	1.97 [15890]	
$K_2NaScF_6:Cr^{3+}$	1.64	1.97					1.97 [15890]	11
$Rb_2KGaF_6:Cr^{3+}$	1.68	1.96 (1.95)	(1.98)	2.84 (2.83)	4.40 (4.40)	0.092 [740]	1.95 [15730]	
$Rb_2KInF_6:Cr^{3+}$	1.64	1.92 (1.92)	(2.25)	2.82 (2.83)	4.40 (4.44)	0.097 [780]	1.92 [15490]	
Tl_2KCrF_6	1.66	1.92 (1.91)	(2.25)	2.82 (2.86)	4.46 (4.44)	0.10 [840]	1.91 [15405]	

[a] The energies in parenthesis correspond to fits of the experimental energies to the calculated energies using the state energy expressions as a function of the Racah parameters B and C, and the crystal-field parameter 10Dq for d^3 configuration. These parameters are given in eV and [cm^{-1}] for C/B = 4.3.

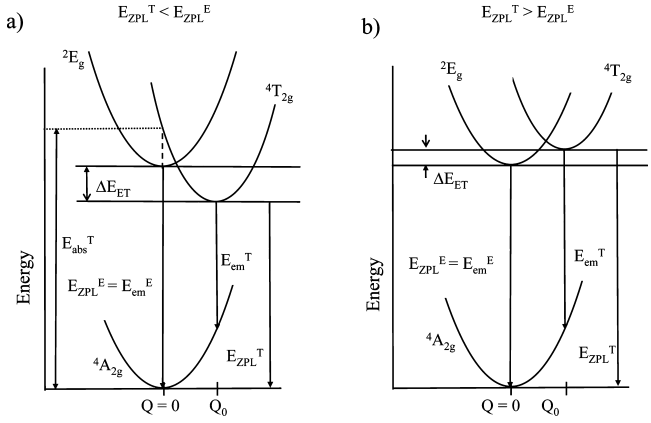

Figure 7. One-coordinate configuration energy curve for the $^4T_{2g}$ and ^2E_g PL excited states and the $^4A_{2g}$ ground state for two different crystal-field values, 10Dq, at the $^4A_{2g}$ equilibrium geometry, above and below the excited-state crossover point. The crossover point is defined as the crossing of zero-phonon-line energies between ^2E_g and $^4T_{2g}$: $\Delta E_{ET} = 0$ with $\Delta E_{ET} = E_{ZPL}(^2E_g) - E_{ZPL}(^4T_{2g})$. The configurational coordinate, Q, of the a_{1g} mode is $Q = 1/\sqrt{6}\sum_{i=1-6}(R_{Cr-Fi} - R^{gr}_{Cr-F})$, where R_{Cr-F_i} and R^{gr}_{Cr-F} are the $Cr-F_i$ distance and the equilibrium distance, respectively.

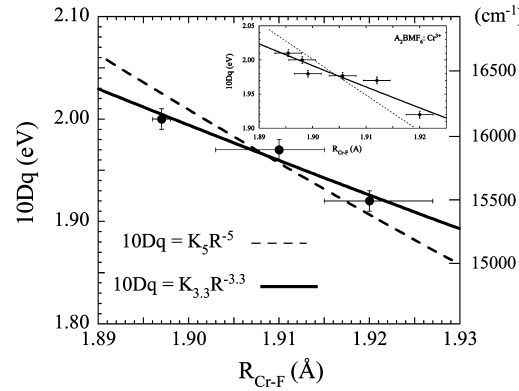

Figure 8. Variation of the crystal field, 10Dq, obtained by fitting from the transition energy, E_1, of the absorption spectra of K_2NaCrF_6, Rb_2KCrF_6, and Tl_2KCrF_6 at ambient conditions with the Cr−F distance given in Table 1. The curves correspond to the equation $10Dq = K_nR^{-n}$ for $n = 5$ and 3.3. The latter exponent corresponds to the best fit to the experimental data. The deviation from $n = 5$ is also illustrated by the variation of 10Dq with R_{Cr-F} along the Cr^{3+}-doped Rb_2KGaF_6, K_2NaGaF_6, and K_2NaAlF_6 series shown in the inset. The local Cr−F distance was derived from the local a_{1g} frequency in the low-temperature emission spectra (Table 1).

The results are compared with R_{Cr-F} dependences of 10Dq given by eq 4 for $n = 5$ and $n = 3.3$. The exponent $n = 3.3$ corresponds to the fit of eq 4 to the experimental data. We associate such a value with the behavior of the first transition energy E_1 around ESCO due to the mixing of $^4T_{2g}(F)$, $^2E_g(G)$, and $^2T_{1g}(G)$ states.

In either case, the R_{Cr-F} values found for the impurity systems from eq 4 are very similar irrespective of the choice $n = 3.3$ or $n = 5$ (Figure 9). It is related to the fact that R_{Cr-F} along the series slightly deviates from the equilibrium Cr−F distance, $R_0 = 1.91$ Å. The method accuracy for determining R_{Cr-F} is confirmed through the good agreement between the bond distances derived from E_1 and those obtained from ab initio calculations[15,58] in $K_2NaGaF_6:Cr^{3+}$ and $K_2NaScF_6:Cr^{3+}$. The calculated host distances are 1.85 and 1.98 Å for Ga−F and Sc−F, while the local Cr−F distances are 1.91 and 1.92 Å for each crystal, respectively. As Figure 9 shows, the R_{Cr-F} derived from eq 4 deviates from R_{M-F} in the $A_2BMF_6:Cr^{3+}$ series as

$$(R_{Cr-F} - R_0) = f(R_{M-F} - R_0) \quad (5)$$

We obtain values of $R_0 = 1.908$ and 1.907 Å, and $f = 0.06$ and 0.09, for $n = 3.3$ and 5, respectively. Equation 5 indicates that there is an important lattice relaxation around Cr^{3+} since R_{Cr-F} deviates from the equilibrium Cr−F distance, $R_0 = 1.908$ Å, only 6% of the deviation of the host M−F distance. Interestingly, the strong relaxation factor, $f = 0.06$, confirms the stiffness of the Cr−F bond in comparison to the more ionic M−F bond, which is probably due to the additional bonding contribution of the 3d orbitals of Cr^{3+}. This result is analogous to findings in Mn^{2+}-doped fluoro- and chloroperovskites, the f values of which are 0.30 and 0.18, respectively.[55] In the latter case, the covalent bonding effect on the lattice relaxation is evidenced by the larger contribution of the Mn−Cl bond with respect to the Mn−F bond.

(58) Luaña, V.; Bermejo, M.; Flórez, M.; Recio, J. M.; Pueyo, L. *J. Chem. Phys.* **1989**, *90*, 6409.

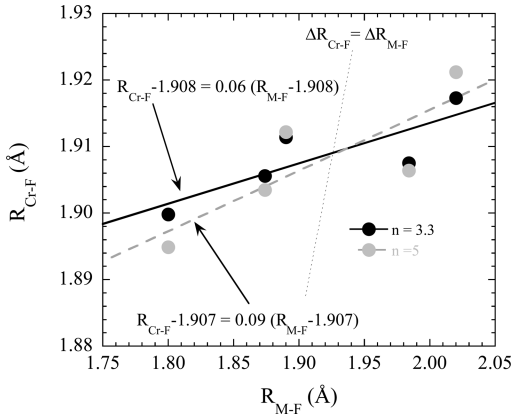

Figure 9. Dependence of the actual Cr−F distance derived from the R_{Cr-F} dependence of 10Dq, which was obtained in the Cr^{3+}-pure fluoroelpasolite crystals, with the M−F distance, R_{M-F}, obtained from X-ray diffraction for the Cr^{3+}-doped fluoroelpasolites given in Table 2. Similar dependences are obtained for any exponent $n = 3.3$ or 5 of the variation $10Dq = K_n R^{-n}$. The linear fits indicate that there is a lattice relaxation around the Cr^{3+} impurity depending on whether $R_{M-F} > R_{Cr-F}$ (inward relaxation) or $R_{M-F} < R_{Cr-F}$ (outward relaxation), R_{Cr-F} being 1.91 Å. The strong lattice relaxation around Cr^{3+} is illustrated by the dotted straight line representing $\Delta R_{M-F} = \Delta R_{Cr-F}$.

Figure 10b shows the variation of the first $^4A_{2g}(F) \rightarrow {}^4T_{2g}(F)$ excitation transition energy, E_1, and the corresponding emission energy, E_{PL}, along the $A_2BMF_6:Cr^{3+}$ series as a function of R_{M-F}. The spectroscopic data for the Cr-pure compounds have been omitted since the emission is probably extrinsic at 300 K and its energy appears additionally red-shifted with respect to the intrinsic PL attained in the Cr^{3+}-doped compounds. One puzzling result is that concerning the unexpected behavior of the PL Stokes shift, $E_S = E_1 - E_{PL}$, with R_{M-F} (Figure 10). E_S increases upon R_{M-F} (or R_{Cr-F}) reduction. This variation is given by $E_S = 0.62 - 0.16R_{M-F}$ (units in eV and Å) and shows an opposite variation of E_S with R observed for Cr^{3+} in chloroelpasolites[23−25] and for Mn^{2+} in chloro- and fluoroperovskites.[12,28,32,54,55] However, a similar variation was found for Ti^{3+} in oxides.[42] This different behavior was explained on the basis of electron−phonon couplings within the complex (MF_6) taking into account contributions from the stronger coupled modes: the totally symmetric a_{1g} mode and the Jahn−Teller e_g mode. Within this model, the Stokes shift is given by $E_S = 2S_{a_{1g}}\hbar\omega_{a_{1g}} + 2S_{e_g}\hbar\omega_{e_g}$.[32] The Huang−Rhys factors associated with these modes, S_{e_g} and $S_{a_{1g}}$, are related to the linear electron−phonon coupling, $A_i = \partial E/\partial Q_i$ with $i = a_{1g}$ and e_g, by the equations

$$S_{a_{1g}} = \frac{A_{a_{1g}}^2}{2\hbar\mu\omega_{a_{1g}}^3} \text{ and } S_{e_g} = \frac{A_{e_g}^2}{2\hbar\mu\omega_{e_g}^3} \qquad (6)$$

where μ, ω, and Q are the reduced mass (the fluorine mass for a_{1g} and e_g), the vibrational frequency, and the normal coordinate of each mode, respectively.[32,24,59] For simplicity, we assume that the vibrational frequency for the ground and excited states is identical. Such an assumption is well justified if we take into account the ratio of excited-state and ground-state vibration frequencies at ambient pressure, $R = \omega_{exc}/\omega_{gr}$, which is 0.997 and 0.97 for the a_{1g} and e_g modes in $(CrF_6)^{3-}$ in fluoroelpasolites, respectively.[15]

Therefore, the R dependence of the Stokes shift can be written as

$$E_S(R_{Cr-F}) = \frac{[A_{a_{1g}}(R_{Cr-F})]^2}{\mu[\omega_{a_{1g}}(R_{Cr-F})]^2} + \frac{[A_{e_g}(R_{Cr-F})]^2}{\mu[\omega_{e_g}(R_{Cr-F})]^2} \qquad (7)$$

The dependence of the electron−vibration coupling on R_{Cr-F} for a_{1g} can be easily obtained from the relation between 10Dq and R_{Cr-F} in eq 4 and considering that the partial derivative with respect to the normal coordinate can be transformed into a partial derivative with respect to R_{Cr-F} by $\partial/\partial Q_{a_{1g}} = (1/\sqrt{6})(\partial/\partial R_{Cr-F})$ in O_h symmetry. Therefore, taking $A_{a_{1g}} = \partial E/\partial Q_{a_{1g}} = (1/\sqrt{6})(\partial 10Dq/\partial R_{Cr-F}) = (-n/\sqrt{6})(KR_{Cr-F}^{-(n+1)})$ and the Grüneisen parameter of the vibrational mode scaled to R_{Cr-F} as $\gamma_{loc} = (1/3)[(\partial \ln \omega_{a_{1g}})/(\partial \ln R_{Cr-F})]$, the a_{1g} contribution to the Stokes shift is thus given by

$$E_s(a_{1g}) = \frac{n^2}{6\mu}\left(\frac{K}{k}\right)^2 R_{Cr-F}^{-2(n+1)+6\gamma_{loc}} \qquad (8)$$

where k is the defined through the relation

$$\omega_{a_{1g}} = kR_{Cr-F}^{-3\gamma_{loc}} \qquad (9)$$

A similar R_{Cr-F} dependence of the Stokes shift is also found for the e_g mode contribution. According to this model, the contribution of the totally symmetric a_{1g} mode to the Stokes shift will either increase or decrease with R_{Cr-F} depending on whether the exponent n (eq 4) is smaller or greater than $3\gamma_{loc} - 1$, respectively. The Grüneisen parameter for the a_{1g} and e_g modes of $K_2NaGaF_6:Cr^{3+}$ is 1.2 and 1.4, respectively.[14,15] However, these values are related to variations of the crystal volume, or the lattice parameter of the elpasolite. Values of $\gamma_{loc} = 2.1$ and 2.5 are obtained if we scale the frequency variation to R_{Cr-F} instead of the lattice parameter. Therefore, we obtain $3\gamma_{loc} - 1 = 5.3$ for the a_{1g} mode, which is significantly bigger than n, and thus E_S should increase with R_{Cr-F}. A similar conclusion is obtained for the e_g coupled mode. This latter conclusion has been experimentally confirmed through the variation of the Jahn−Teller energy, $E_{JT} = S_{e_g}\hbar\omega_{e_g}$, derived from the spin−orbit reduction in the $^4T_{2g}$ state (Ham effect) measured in Cr^{3+}-doped Cs_2NaMCl_6 (M = Sc, In, and Y).[23,24] Besides the increase of E_S with R_{M-Cl}, the contribution of the e_g mode to E_S, which is known through E_{JT}, also increases along the series 36.7 meV ($R_{Sc-Cl} = 2.49$ Å), 38.5 meV ($R_{In-Cl} = 2.51$ Å), and 41.0 meV ($R_{Y-Cl} = 2.56$ Å).[24,25]

Nevertheless, this model does not account for the anomalous decreases of the Stokes-shift variation with R_{Cr-F}, which is observed in the present work (Figure 10). Whereas the ab initio calculated E_S increases from 0.25 to 0.26 eV[14] on passing from K_2NaGaF_6 ($R_{Ga-F} = 1.88$ Å) to K_2NaScF_6 ($R_{Sc-F} = 1.98$ Å), the experimental E_S decreases, $\delta E_S = -7$ meV. This experimental trend, which is clearly confirmed along with the wide Cr-doped elpasolite series shown in Figure 10, is associated with the presence of Fano resonances in the first excited state. Such an effect is responsible for the tripletlike structure of the first OA band and thus the

(59) Henderson, B.; Imbusch, G. F. *Optical spectroscopy of inorganic solids*; Clarendon Press: Oxford, 1989.

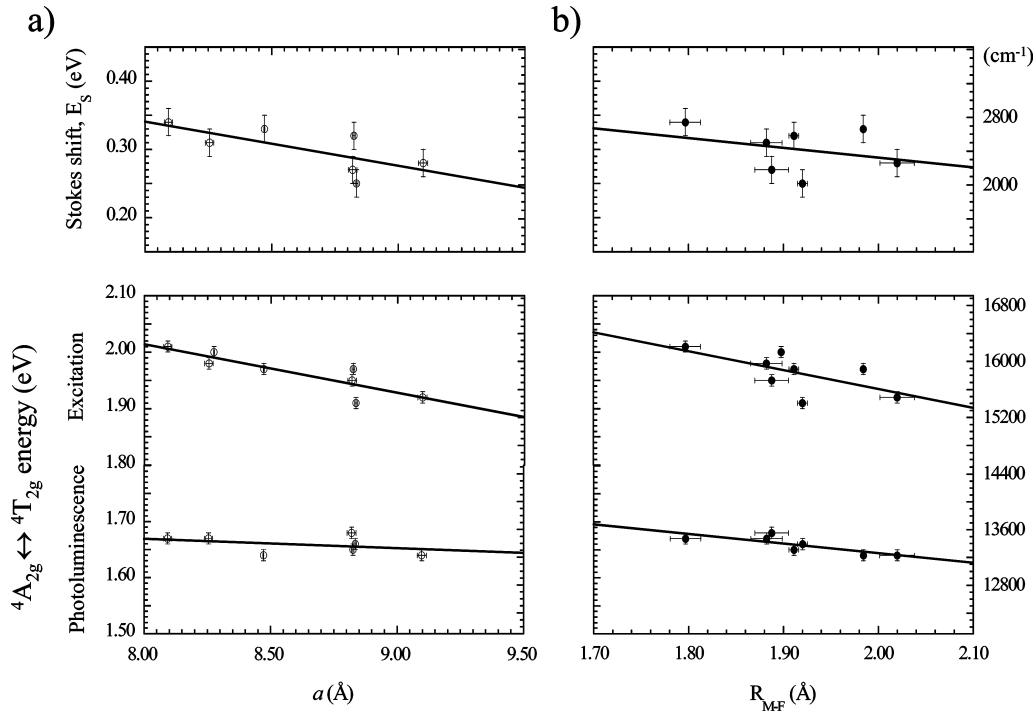

Figure 10. (a) Variation of the first excitation energy, E_1; the PL energy, E_{PL}; and the Stokes shift, $E_S = E_1 - E_{PL}$, with the lattice parameter, a. (b) Variation with the M−F bond distance, R_{M-F}, in the Cr^{3+}-pure and Cr^{3+}-doped A_2BMF_6 series. Data are collected in Tables 1 and 2. Open and closed circles denote experimental points represented as a function of a and R_{M-F}, respectively.

different R-induced shift of E_1 and E_{PL} in comparison to those Cr^{3+} systems, whose CF is quite separate from ESCO, $(10Dq/B)_{ESCO} \approx 20$. In fact, the electronic structure calculations performed on $(CrF_6)^{3-}$ provide E_S values which refer to the $^4T_{2g}$ excited state yet exclude the resonant effect with the ^2E and $^2T_1$ states. The so-obtained E_S variation coincides with that predicted by the complex model given above but is unable to account for the experimental variation shown in Figure 10.

The understanding of how E_1 and E_{PL} depend on R_{M-F} is crucial to explaining the Stokes-shift variation, δE_S. $|\delta E_1| > |\delta E_{PL}|$ in Cr^{3+} fluoroelpasolites, but it is worth noting that such behavior is contrary to the general trend observed for Cr^{3+} in chlorides, $|\delta E_1| < |\delta E_{PL}|$, given that the variation of E_1 with 10Dq is positive. If $\partial E/\partial 10Dq$ was negative, then $|\delta E_1| > |\delta E_{PL}|$, as occurs for Mn^{2+}.[32,54,55] It must be noted that in both situations $\partial E_S/\partial 10Dq = \partial(E_1 - E_{PL})/\partial 10Dq < 0$. We ascribe the anomalous variation of E_{PL} with respect to E_1 for positive $\partial E/\partial 10Dq$ and, thus, E_S in $(CrF_6)^{3-}$ to the ESCO. The PL state mainly corresponds to the lowest-energy state of the manifold $^4T_{2g}$, ^2E_g, and $^2T_{1g}$ mixed states by the spin−orbit interaction (Figure 3b). Given that the energy splitting is maximum at ESCO, we expect a weaker blueshift contribution to E_{PL} with increasing 10Dq (or decreasing R_{Cr-F}) as the PL state approaches ESCO. The reduction of δE_{PL} with 10Dq with respect to δE_1 due to this effect may lead to an increase in E_S with 10Dq (or decrease with R_{M-F}) as observed in Figure 10. Therefore, we suggest that ESCO can be responsible for the decrease of E_S with R_{Cr-F} in Cr^{3+} in fluoroelpasolites, as a consequence of the slightly weaker R dependence of E_{PL} than E_1.

C. High-Pressure Spectroscopy in Rb_2KCrF_6. High-pressure experiments carried out on Rb_2KCrF_6 enable us to confirm the present model and verify whether R dependences of the Stokes shift induced either by chemical pressure or by external pressure are equivalent. Figure 11 plots the variation of the Rb_2KCrF_6 PL and excitation spectra with pressure at room temperature. The main feature is the blue shift of 0.09 eV experienced by the PL band with increasing pressure in the 0−7 GPa range, in agreement with the increase of 10Dq upon R_{Cr-F} reduction. Above this pressure, the band maximum is located around 1.81 eV, and sharp features appear at 1.835, 1.865, and 1.895 eV. The peak at 1.865 eV corresponds to the mainly $^2E_g(G) \rightarrow {}^4A_{2g}(F)$ ZPL, while the other two peaks are the Stokes and anti-Stokes phonon replicas associated with the t_{2u} vibrational mode of 30 meV, respectively. A similar result was first found by Dolan et al.[11] in the emission spectrum of $K_2NaGaF_6:Cr^{3+}$ at $T = 154$ K and $P = 6.1$ GPa.

The change of slope in the pressure dependence of PL energy at 7 GPa observed in Figure 5 reveals that ESCO occurred near this point. The PL lifetime increases with pressure from $\tau = 45$ μs (ambient pressure) to $\tau = 1.0$ ms (16.5 GPa), as is shown in the inset of Figure 6. This variation confirms the occurrence of the ESCO phenomenon. According to the normal-coordinate configuration diagram of Figure 7, ESCO actually takes place when the ZPL energy of $^4T_{2g}$ and ^2E_g coincides: $E_{ZPL}(^4T_{2g}) = E_{ZPL}(^2E_g)$. From the estimated ZPL for $^4T_{2g}$ and the observed band shifts, the variation of the ZPL-energy difference with pressure is given by $\Delta(P) = E_{ZPL}(^4T_{2g}) - E_{ZPL}(^2E_g) = 0.013P - 0.065$, and thus ESCO takes place at 5 GPa. The presence of broadband emission above the ESCO pressure at 7 GPa reflects the thermal population of the $^4T_{2g}(F)$ state. The oscillator strength for the spin-allowed $^4A_{2g}(F) \rightarrow {}^4T_{2g}(F)$ transition is about an order of magnitude greater than the spin-forbidden $^2E_g(G)$

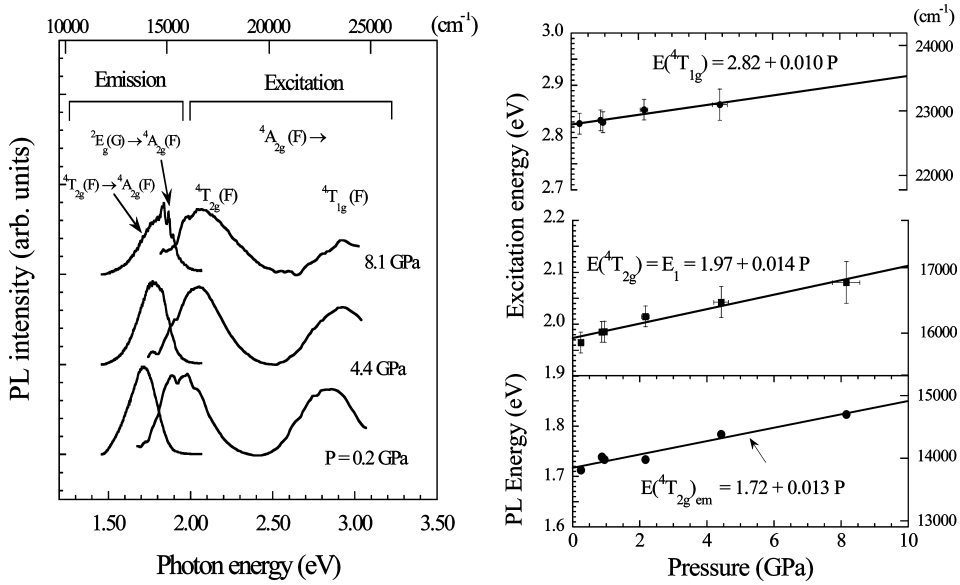

Figure 11. (a) Pressure dependence of the excitation and emission spectra of Rb_2KCrF_6 at room temperature. Note the presence of sharp features associated with the $^2E_g \rightarrow {}^4A_{2g}$ emission at 8.1 GPa. (b) Variation of the $^4T_{1g}$ and $^4T_{2g}$ excitation energies, and the corresponding PL band energy. The straight lines correspond to the least-squares linear fits of $E(P)$ data. Note that the Stokes shift, $E_s = E_1 - E_{PL}$, slightly increases with pressure at a rate of 1 meV/GPa.

$\rightarrow {}^4A_{2g}(F)$ one, and therefore the broadband emission still dominates the PL spectrum at the ESCO pressure and even at higher pressures, although the $^4T_{2g}(F)$ state is well above the $^2E_g(G)$ state.

Taking an oscillator-strength ratio of 20, then the two transitions would then display similar intensities for an energy separation $\Delta = E_{ZPL}({}^4T_{2g}) - E_{ZPL}({}^2E_g) = k_BT(\ln 12)$, which is 64 meV for $T = 300$ K. In this estimate, we have considered that the state degeneracy for $^4T_{2g}$ and ^2E_g are 12 and 4, respectively. That condition is fulfilled at around 10 GPa (5 GPa above the ESCO pressure) if we use the pressure dependence of the $^4T_{2g}$ energy given by $\partial E_{ZPL}({}^4T_{2g})/\partial P =$ 13 meV/GPa (Figures 7 and 11). This pressure reduces to 6 GPa working at $T = 60$ K, and therefore ESCO is easily observed at low temperatures.[1,11,25] The $\tau(P)$ variation and the PL spectral evolution depicted in Figure 6 agree with the proposed scenario. It must be noted that the calculated variation of $\tau(P)$ employs a crystal-field model without considering explicitly the spin−orbit interaction. Although the spin−orbit-induced state mixing between $^4T_{2g}$ and ^2E_g plays a role in the pressure dependence of the lifetime in the low-temperature regime, it can be shown that that both the spin−orbit quantum model[1] and the classical model provide, within 1% precision, the same pressure dependence of $\tau(P)$ if the spin−orbit coupling constant, ζ, obeys $\zeta \leq k_BT$.[60] This condition is fulfilled for Cr^{3+} in fluoroelpasolites ($\zeta \approx 200$ cm^{-1})[10,20] at $T = 300$ K, and thus lifetime and spectral data can be easily correlated through the present model.

Figure 11b plots the variation of the emission and the first excitation energy as a function of pressure. As observed in the fluoroelpasolite series, both E_1 and E_{PL} shift to higher energies with increasing pressure, the emission blue shift being smaller than the excitation blue shift ($\delta E_{PL} < \delta E_1$). It must be remarked that the overall pressure variation leads us to expect an increase in the Stokes shift, as occurs along the series. Furthermore, the measured shift rates of 14 meV/GPa for excitation and 13 meV/GPa for emission can be reconciled with findings along the series if we use a local bulk modulus for $(CrF_6)^{3-}$ in elpasolites of $K_0 = 110$ GPa.[15] In fact, the pressure variation of E_1 is given by

$$\left(\frac{\partial E_1}{\partial P}\right)_T = \frac{\partial E_1}{\partial R_{Cr-F}}\left(\frac{\partial R_{Cr-F}}{\partial P}\right)_T = \frac{\partial E_1}{\partial R_{Cr-F}}\frac{R_{Cr-F}}{3K_0} \qquad (10)$$

Using eqs 4 and 10, we finally obtain

$$\left(\frac{\partial E_1}{\partial P}\right)_T = \frac{nE_1}{3K_0} \qquad (11)$$

Taking $n = 3.3$, we estimate a variation of E_1 with P of 19 meV/GPa, which is in agreement with the measured values. This result contrasts with estimates based on an exponent $n = 4.5$ and a bulk modulus for fluoroelpasolites, $K_0 \approx 49$ GPa.[34] From those values, we obtain a variation of 57 meV/GPa, which is almost a factor of 5 greater than the experimental variation of 14 meV/GPa. Therefore, the pressure results confirm that the PL properties and main spectral features of Cr^{3+}-doped fluoroelpasolites can be explained on the basis of a $(CrF_6)^{3-}$ complex, the variation of which is governed by the actual Cr−F bond distance imposed by the host crystal. It should be noted that Rb_2KCrF_6 and Rb_2KGaF_6 transform at low temperature (below 153 and 123K, respectively) into an original structural type.[61] The main originality of the structure concerns the environment of 4/5 of the potassium atoms (B sublattice) which are transformed from octahedra into pentagonal bipyramids

(60) Hernández, I. Ph. D. Thesis, University of Cantabria, Santander, Spain, 2006.

(61) Zúñiga, F. J.; Tressaud, A.; Darriet, J. *J. Solid State Chem.* **2006**, *179*, 3607.

sharing edges with adjacent MF_6 octahedra containing Cr or Ga. The displacive phase transition can be explained straightforwardly by the rotation of 45° in the (a,b) plane of 1/5 of the MF_6 (M = Cr, Ga) octahedra.

IV. Conclusions

Throughout this work, we show the following: (1) The local structure around the impurity in Cr^{3+}-doped elpasolites can be derived from the corresponding optical spectra after structural correlation established in Cr^{3+}-pure elpasolite series. (2) The *R* dependences of 10Dq and the Stokes shift exhibit anomalous deviations with respect to crystal-field model expectations, due to the state mixing of the first absorption band of Cr^{3+}. The weak *R* dependence of E_1 (10Dq) as $E_1 = KR^{-3.3}$ and the increase of E_S upon *R* reduction, or increasing pressure, are both explained on this basis. The unusually small exponent $n = 3.3$ is interpreted as being due to resonance effects associated with $^2E_g(G)$, $^2T_{1g}(G)$, and $^4T_{2g}(F)$ in the crystal field of Cr^{3+} attained in fluoroelpasolites. (3) The PL properties along the elpasolite series or as a function of pressure can be understood from the $(CrF_6)^{3-}$ complex, whose actual Cr−F distance is mainly governed by either the host crystal or the external pressure. We have demonstrated that there is a strong lattice relaxation around Cr^{3+} in Cr-doped elpasolites yielding either an inward or an outward relaxation of the fluorine octahedron depending on whether the host M−F distance is longer or shorter than $R_{Cr-F} = 1.903$ Å. (4) The $^2E_g(G) \leftrightarrow {}^4T_{2g}(F)$ excited-state crossover takes place in Rb_2KCrF_6 around 7 GPa. However, this effect is not confirmed by the presence of sharp features at 7 GPa but about 12 GPa at room temperature. This pressure provides enough energy separation between $^4T_{2g}(F)$ and $^2E_g(G)$ to increase the population of the long-lived $^2E_g(G)$ state with respect to the short-lived $^4T_{2g}(F)$ state at room temperature according to their respective transition rates. The present results indicate that the selected $A_2BMF_6:Cr^{3+}$ crystals are suitable systems to establish structural correlations between PL and R_{Cr-F}.

Acknowledgment. The authors thank Cyril Allegret for his collaboration in the experimental work. Financial support from the Spanish Ministerio de Educación y Ciencia (Project No. MAT2005-00099) is acknowledged. I.H. and F.R. also wish to offer their thanks for partial support from the Research Intensification program (I3) of the University of Cantabria. This work has been carried out within the framework of the MALTA Consolider Ingenio 2010 program (CSD2007-00045).

This paper is dedicated to the memory of Neil Bartlett, who passed away August 2008, in recognition of his outstanding contributions across a broad spectrum of fluorine chemistry.

IC800606H